

Constitutive Modelling of Lamb Aorta

Ryley A. Macrae, Jane Pillow, Karol Miller, and Barry J. Doyle

1 Introduction

Vascular inflammation is an established marker of cardiovascular pathogenesis, but its role on arterial tissue biomechanics is not well understood. Inflammation has been identified as a risk factor for many adverse cardiovascular events [1], and is associated with increased risk even in apparently healthy individuals [2]. Inflammation is now widely regarded as a major contributing factor in the pathogenesis

R.A. Macrae

Vascular Engineering Laboratory, Harry Perkins Institute of Medical Research, Perth, WA, Australia

Intelligent Systems for Medicine Laboratory, School of Mechanical and Chemical Engineering, The University of Western Australia, Perth, WA, Australia

J. Pillow

School of Human Sciences, University of Western Australia, Australia

Centre for Neonatal Research and Education, School of Medicine, University of Western Australia, Australia

K. Miller

Intelligent Systems for Medicine Laboratory, School of Mechanical and Chemical Engineering, The University of Western Australia, Perth, WA, Australia

Institute of Mechanics and Advanced Materials, Cardiff University, Cardiff, UK

B.J. Doyle (✉)

Vascular Engineering Laboratory, Harry Perkins Institute of Medical Research, Perth, WA, Australia

British Heart Foundation Centre for Cardiovascular Science, The University of Edinburgh, Edinburgh, UK

School of Mechanical and Chemical Engineering, The University of Western Australia, Perth, WA, Australia

e-mail: Barry.Doyle@uwa.edu.au

of atherosclerosis [3, 4]. The inflammatory process is also associated with the development of aneurysms [5]. Furthermore, aneurysms with acute inflammation have been demonstrated to exhibit an increased rate of expansion [6–8].

These diseases involve extensive vascular remodelling changes to tissue biomechanics, but outside of gross changes to artery behaviour little work has been done on isolating the effect of inflammation on tissue biomechanics. There is a wealth of literature associating the presence of both acute and chronic inflammation with increased arterial stiffness as indicated by in-vivo measurements such as pulse-wave velocity (PWV) [9–12] but the mechanisms behind this remain unclear. Furthermore, while measurements such as pulse-wave velocity can illustrate the gross behaviour of arterial biomechanics under physiologic loading conditions, the precise effects of inflammation on the biomechanics of arteries remain relatively unexplored. The use of liposaccharides as a means for producing animal models of inflammation is well established. Intra-amniotic delivery of LPS to the fetus is widely used to model perinatal inflammation, though very few studies have examined the effect of this inflammation on cardiovascular biomechanics; though induced perinatal inflammation has been shown to alter haemodynamics and induce structural changes in the heart and small vessels [13–20].

The development of reliable constitutive models of the artery is necessary in order to better comprehend the mechanical component of cardiovascular disease pathogenesis [21], as well as providing insight into the complex biomechanical behaviours induced during therapeutical interventions such as arterial clamping and angioplasty [22]. The aim of this project was to develop constitutive models for the aorta of LPS-treated and non-treated lambs, so as to assess the impact of perinatal inflammation on arterial biomechanics. Changes in the arterial stiffness can lead to arterial remodelling and dysfunction, and so its characterization can provide insight into the nature of inflammatory processes, as well as being used to describe long term changes in arterial structure due to active vascular remodelling processes.

2 Methods

2.1 Subjects

Intra-amniotic LPS has been shown to impact the cardiovascular development of mouse [23] and rat [13] animal models, as well as impair function, alter the heart structure and induce expression of the inflammatory markers cytokine interleukin-1B and tumour necrosis factor in the myocardium of sheep [18, 24]. Foetal lambs were exposed to intra-amniotic injections of either saline (control group $n = 4$) or 4 mg *Escherichia coli* LPS (2 mg/mL: Sigma-Aldrich; 055:B5) (LPS group, $n = 6$) 2 days prior to operative preterm delivery at 129 days gestation. Lambs were then ventilated for 7 days, and then euthanized via 150 mg/kg of intravenous pentobarbitone (Valbarb, Jurox, Australia) for post-mortem. The aortas from each preterm lamb were excised for mechanical testing.

2.2 Test Protocol

Due to the small size of the excised specimens, mechanical testing was conducted via uniaxial loading of a ring-shaped specimen with a custom-built uniaxial test rig. While uniaxial tension experiments are insufficient to fully characterize the three-dimensional constitutive stress–strain relations of biological materials, these tests can provide useful descriptive information of the mechanical behaviour [25].

Testing was conducted within 24 h of excision. Ring-shaped samples were prepared by cutting the tubular specimen (i.e. the aorta) into smaller sections of an approximate width of 1.5 mm via circumferential cuts normal to the central axis (average of 8 rings per aortic specimen). Wall thickness (mean = 1.01 mm), sample width (mean = 1.58 mm) and ring circumference (mean = 12.8 mm) were measured optically via ImageJ. Average wall thickness was taken as the mean of 8 measurements, average wall width taken as the mean of 5 measurements and vessel circumference measured directly with the measurement tool. The sample was then mounted between two parallel metal wires and pre-stretched to the configuration shown in Fig. 1 and preconditioning applied via loading–unloading cycles until a repeatable displacement–force curve was obtained, as is standard for uniaxial testing of biological soft tissues [26]. Preconditioning was conducted to a maximum strain of 0.2 in all samples, and a repeatable mechanical response was noted after five loading–unloading cycles. Before testing, images of the sample were again taken to measure the initial distance between the pins (as shown in Fig. 1).

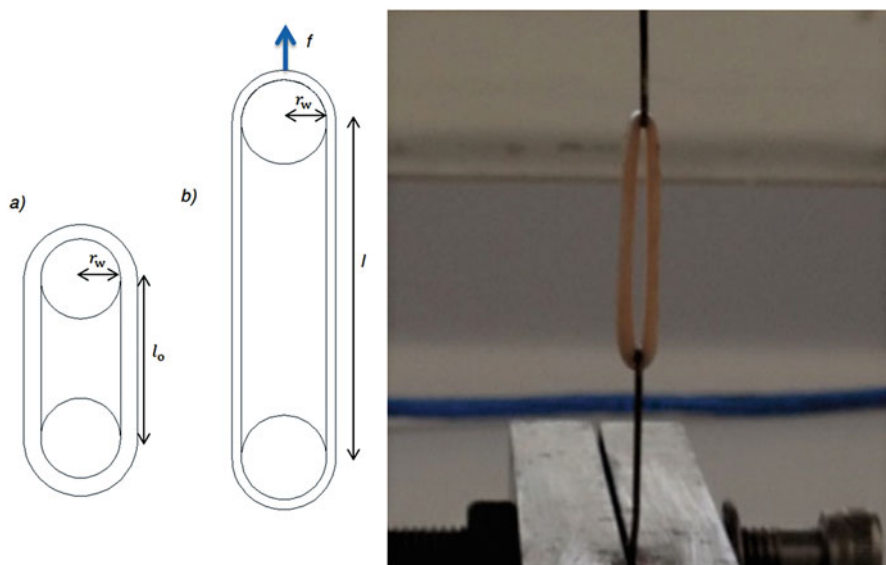


Fig. 1 Schematic of a uniaxial tension test of an arterial ring in the (a) reference and (b) deformed configuration, and corresponding photograph of loaded specimen. Reproduced from [25]

The approximate strain is calculated by measuring the displacement between the two wires [27, 28]. The average stretch ratio in the circumferential direction $\lambda_{\theta\text{avg}}$ is most simply determined by:

$$\lambda_{\theta\text{avg}} = \frac{l + \pi r_w}{l_o + \pi r_w} \quad (1)$$

where r_w is the radius of the cylindrical wire and l and l_o are the distances between the centres of the wires. Wires were coated in oil so as to minimize friction at the boundaries, and stress induced by friction was neglected from the analysis. The sample was then extended at a constant rate of 0.1 mm/s until failure whilst continuously measuring displacement and force.

2.3 Data Analysis

As the constitutive relations derived are intended to describe the mechanical behaviour and allow for comparison between LPS-treated and control specimens, data was processed in terms of the global stretch ratio consistently across specimens [29]. It was assumed that the effects of any friction and bending stiffness would be either negligible or relatively consistent across samples. Upon pre-loading the sample force was noted to be approximately 0.01 N, as compared to an average failure force of 2 N, indicating that the effect of bending stiffness was relatively low. Thus, assuming the ring is free to move along the wire boundary, nominal stress (S_{avg}) will be given by:

$$S_{\text{avg}} = \frac{F_{\text{exp}}}{2 \cdot A_{\text{avg}}} \quad (2)$$

where A_{avg} is the average cross-sectional area of the ring, assumed to be rectangular, $A_{\text{avg}} = t \cdot w$, and F_{exp} is the measured tension. However, while the width of each ring could be assumed constant, wall thickness around the ring was shown to vary significantly, with some rings showing a variation in wall thickness up to 30%. Thus, the assumption of constant cross-sectional area throughout the ring is invalid. Assuming the ring breaks at the smallest cross-sectional area, with the data of specimens which broke near the wires or in a region distinct from that of lowest cross-sectional area discarded, the nominal stress at the smallest cross-sectional area (S_b) can be determined from experimental data via:

$$S_{b\text{exp}} = \frac{F_{\text{exp}}}{2 \cdot A_b} \quad (3)$$

where A_b is the smallest initial cross-sectional area, as calculated at the smallest thickness. In order to derive a stress–strain relationship, it is necessary to relate the global average stretch (λ_{avg}) to a stretch local to the point of failure (λ_b). Assuming

circumferential force (F_θ) is constant throughout the ring, circumferential stress will be proportional to the initial cross-sectional area:

$$F_\theta = S_{\text{avg}} \cdot A_{\text{avg}} = S_b \cdot A_b \quad (4)$$

If we assume isotropy and incompressibility, the strain energy function can be expressed in terms of the first and second invariants of the Green strain tensor [30]:

$$W = \bar{W}(I_1, I_2) \quad (5)$$

Assuming no shear, under uniaxial tension the strain invariants are given by:

$$I_1 = \lambda_1^2 + \frac{2}{\lambda_1}, \quad I_2 = 2\lambda_1 + \frac{1}{\lambda_1^2} \quad (6)$$

where λ_1 is the stretch in the direction of loading λ_θ . An Ogden model [31] with $N = 1$ proved a good fit ($R^2 \geq 0.97$) for the data while utilizing few parameters, given as follows:

$$W = \frac{\mu}{\alpha} (\lambda_1^\alpha + \lambda_2^\alpha + \lambda_3^\alpha - 3) \quad (7)$$

With nominal stress being given by:

$$S_1 = \frac{\mu}{\lambda_1} \left(\lambda_1^\alpha - \lambda_1^{-\frac{\alpha}{2}} \right) \quad (8)$$

where $[\mu, \alpha]$ are the particular coefficients of a given strain energy function. For the given strain levels, the use of higher order models is not warranted, as indicated by the goodness of fit. Determining the stretch ratio at the region of smallest cross-sectional area (λ_b) is a not entirely trivial matter. In this particular case, λ_b was determined via substituting Eq. (8) into the relation given by Eq. (4), such that:

$$\frac{(\lambda_b^\alpha - \lambda_b^{-\frac{\alpha}{2}})}{\lambda_b} = \frac{A_{\text{avg}}}{A_b} \cdot \frac{(\lambda_{\text{avg}}^\alpha - \lambda_{\text{avg}}^{-\frac{\alpha}{2}})}{\lambda_{\text{avg}}} \quad (9)$$

For the given measurements of A_b , A_{avg} and the range of values determined from displacement data $[\lambda_{\text{avg}}]$, an initial guess was made of the constitutive parameters $[\mu, \alpha]$ and used to compute corresponding local stretch values $[\lambda_b]$. These values of stretch were then used to compute S_b as per Eq. (8). Model calibration was conducted via minimizing the error between this curve $S_b - \lambda_b$ and the curve derived from experimental data $S_{\text{bexp}} - \lambda_b$, as determined from Eq. (3). Error was computed via a least squares method weighted towards the low-strain region:

$$\text{Error} = \sum \left(1 - \frac{S_{\text{model}}}{S_{\text{exp}}} \right)^2 \quad (10)$$

Error was weighted towards the low stress/strain region, as data in this region is of more physiological relevance than that in the very high strain region. In addition, data in the high stress–strain region is also influenced by factors not accounted for in the model, such as tissue damage occurring prior to tissue failure. The resultant fitted parameters $[\mu, \alpha]$ were then used to compute a new local stretch as described above which was then input into Eq. (9), and this approach iterated until successive error between computed constitutive parameters was negligible. All model calibration was conducted via a custom MATLAB script. While initial guesses for the constitutive parameters were at first selected arbitrarily, to reduce calibration time the initial guesses were then set to values approximate to those determined for early samples; $[\mu = 2 \times 10^{-4}, \alpha = 10]$.

Shear modulus in the undeformed state was derived from the Ogden model via:

$$\mu_o = \frac{1}{2}\mu\alpha \quad (11)$$

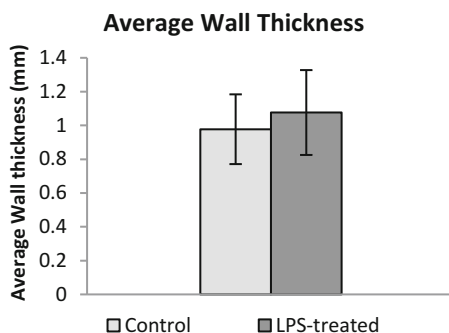
3 Results

Data from ten specimens (cut into approximately eight rings each) were utilized (control $n = 4$, LPS-treated $n = 6$). LPS-treated lambs demonstrated a trend towards higher wall thickness, though this finding was not significant ($p > 0.35$), with aortic specimens from the control group having an average of thickness of 0.977 ± 0.073 mm and LPS-treated group 1.076 ± 0.079 mm (see Fig. 2).

Force-extension data of rings cut from a single specimen showed high consistency (Fig. 3). Incorporation of the local stretch as determined by Eq. (9) affected the estimates of the Ogden parameter μ by up to 15%, and had no appreciable effect on determination of the parameter α ($\leq 0.1\%$). Fig. 4 illustrates the stress-stretch curve as assessed by taking a constant cross-sectional area compared to the stress-stretch curve computed with a locally determined stretch, for a representative sample.

The average constitutive parameters determined for the Ogden model were not significantly different between groups (see Table 1, Fig. 5), although μ

Fig. 2 Average wall thicknesses of the aorta for both the control and LPS-treated groups with standard deviations



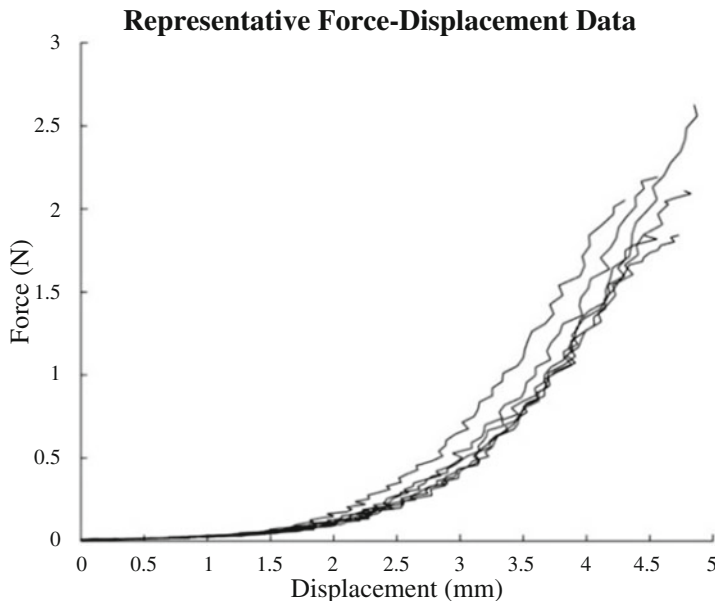


Fig. 3 Experimental force–displacement curves taken from a representative specimen (LPS-treated)

trended higher in the LPS-treated group ($\mu = 7.77 \times 10^{-4} \pm 6.96 \times 10^{-4}$ versus $4.43 \times 10^{-4} \pm 3.67 \times 10^{-4}$; $p > 0.4$). The α parameter showed no difference between groups ($p > 0.85$), with an average of 12.78 ± 0.58 MPa (control = 12.96 ± 2.145 , LPS-treated = 12.65 ± 3.378). A difference was noted in the initial shear modulus, being higher in the LPS-treated group ($4.48 \times 10^{-3} \pm 3.71 \times 10^{-3}$ MPa versus $2.70 \times 10^{-3} \pm 2.23 \times 10^{-3}$ MPa), although again variation was high and the finding was non-significant ($p > 0.4$).

4 Discussion and Conclusion

The relation between inflammation and cardiovascular disease is widely researched, yet little data exists on the biomechanical impact of inflammation on the aorta. Previous studies suggest that inflammation stiffens the aorta [32, 33]; however, these previous studies use in-vivo pulse-wave velocity with inherent assumptions on aortic morphology, and not physical biomechanical ex-vivo testing. Our preliminary ex-vivo data suggests that LPS-induced systemic inflammation during foetal development does not greatly affect the biomechanical behaviour (i.e. stiffness) of the aorta, as assessed by vessel constitutive parameters. The development of these constitutive models provides valuable data on the precise

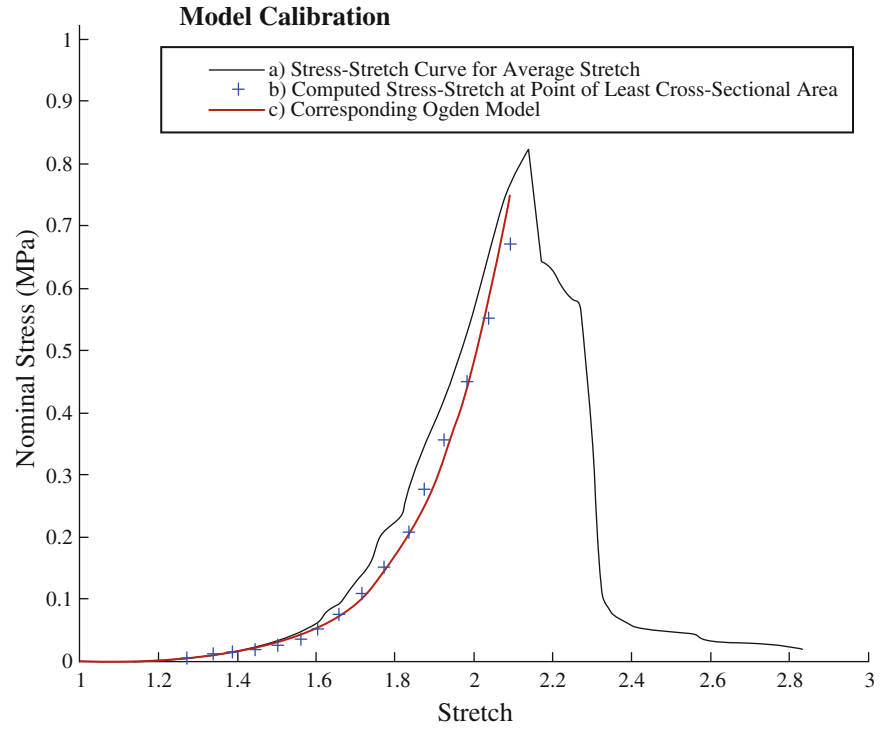


Fig. 4 Representative stress-stretch curves from a single sample (LPS-treated): **(a)** stress-stretch curve derived from the average stretch throughout the ring specimen; **(b)** stress-stretch curve at the smallest cross-sectional area as computed during model calibration and **(c)** the Ogden model fit to the computed stress-stretch curve at smallest cross-sectional area

Table 1 Collected values of constitutive parameters and initial shear modulus. Statistical significance was not reached in any case

Group	–	μ (MPa)	α	μ_o (MPa)
Control	Mean	4.43×10^{-4}	12.96	2.70×10^{-3}
	Standard Dev	$\pm 3.67 \times 10^{-4}$	± 2.145	$\pm 2.23 \times 10^{-3}$
LPS-treated	Mean	7.77×10^{-4}	12.65	4.48×10^{-3}
	Standard Dev	$\pm 6.96 \times 10^{-4}$	± 3.378	$\pm 3.71 \times 10^{-3}$

effects on mechanical behaviour of perinatal inflammation. Although there was on average a trend for LPS-treated arteries to be stiffer in the low-strain region, a significant change in stiffness expected was not demonstrated. The majority of prior studies employ pulse-wave velocity as an indicator of bulk stiffness, and thus care must be taken when comparing this data to the material stiffness given by the elastic modulus as measures of bulk stiffness are dependent on the thickness of the artery [34].

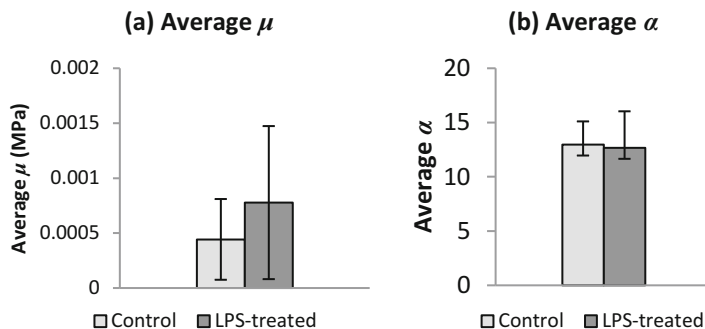


Fig. 5 Average constitutive parameters (a) μ and (b) α computed for both LPS-treated and control groups, with standard deviation

There are limitations to our work and it is possible the induced systemic inflammation was insufficiently present in the foetal cardiovascular system—either in severity or duration—to provoke a significant change in the biomechanics of the aorta. The constitutive parameters determined are primarily intended for comparison between treatment groups, and thus have not taken into account the potential impact of boundary friction on the parameter values. For a more precise determination of constitutive parameters, finite element method should be used [35]. The study was further limited by the number of specimens; due to the high variability in material properties between subjects, more data would be required to ascertain what, if any, correlation exists between systemic foetal inflammation and arterial biomechanics. This data represents a preliminary cohort, with testing of additional subjects currently underway. As this article is focussed on assessing the passive biomechanical response of the artery as an indication of structural remodelling, it necessarily neglects the active response of the artery, largely mediated via nitric oxide production [10].

In conclusion, this is the first study to assess the impact of inflammation on the biomechanical response of the aorta, using ex-vivo test methods. We show that in our preliminary cohort, inflammation does not significantly impact aortic stiffness, and the preterm lamb can be represented by a first order Ogden constitutive model. Further testing is needed to conclusively determine the effect of inflammation on aortic biomechanics.

References

1. Bhatt DL, Topol EJ (2002) Need to test the arterial inflammation hypothesis. *Circulation* 106(1):136–140
2. Rohde LE, Hennekens CH, Ridker PM (1999) Survey of C-reactive protein and cardiovascular risk factors in apparently healthy men. *Am J Cardiol* 84(9):1018–1022
3. Libby P (2002) Inflammation in atherosclerosis. *Nature* 420(6917):868–874

4. Ross R (1999) Atherosclerosis—an inflammatory disease. *N Engl J Med* 340(2):115–126
5. Rasmussen TE, Hallett JW Jr, Schulte S, Harmsen WS, O’Fallon WM, Weyand CM (2001) Genetic similarity in inflammatory and degenerative abdominal aortic aneurysms: a study of human leukocyte antigen class II disease risk genes. *J Vasc Surg* 34(1):84–89
6. Mosorin M, Juvonen J, Biancari F, Satta J, Surcel HM, Leinonen M, Saikku P, Juvonen T (2001) Use of doxycycline to decrease the growth rate of abdominal aortic aneurysms: a randomized, double-blind, placebo-controlled pilot study. *J Vasc Surg* 34(4):606–610
7. Pyo R, Lee JK, Shipley JM, Curci JA, Mao D, Ziporin SJ, Ennis TL, Shapiro SD, Senior RM, Thompson RW (2000) Targeted gene disruption of matrix metalloproteinase-9 (gelatinase B) suppresses development of experimental abdominal aortic aneurysms. *J Clin Invest* 105(11):1641–1649
8. Richards JM, Semple SI, MacGillivray TJ, Gray C, Langrish JP, Williams M, Dweck M, Wallace W, McKillop G, Chalmers RT, Garden OJ, Newby DE (2011) Abdominal aortic aneurysm growth predicted by uptake of ultrasmall superparamagnetic particles of iron oxide: a pilot study. *Circ Cardiovasc Imaging* 4(3):274–281
9. Aznaouridis KA, Stefanadis CI (2007) Inflammation and arterial function. *Artery Research* 1(1):32–38
10. Jain S, Khera R, Corrales-Medina VF, Townsend RR, Chirinos JA (2014) Inflammation and arterial stiffness in humans. *Atherosclerosis* 237(2):381–390
11. Mäki-Petäjä KM, Wilkinson IB (2012) Inflammation and large arteries: potential mechanisms for inflammation-induced arterial stiffness. *Artery Res* 6(2):59–64
12. Park S, Lakatta EG (2012) Role of inflammation in the pathogenesis of arterial stiffness. *Yonsei Med J* 53(2):258–261
13. Abdulkadir AA, Kimimasa T, Bell MJ, MacPherson TA, Keller BB, Yanowitz TD (2010) Placental inflammation and fetal hemodynamics in a rat model of chorioamnionitis. *Pediatr Res* 68(6):513–518
14. Galinsky R, Hooper SB, Wallace MJ, Westover AJ, Black MJ, Moss TJ, Polglase GR (2013) Intrauterine inflammation alters cardiopulmonary and cerebral haemodynamics at birth in preterm lambs. *J Physiol* 591(8):2127–2137
15. Kallapur SG, Bachurski CJ, Cras TDL, Joshi SN, Ikegami M, Jobe AH (2004) Vascular changes after intra-amniotic endotoxin in preterm lamb lungs. *Am J Phys Lung Cell Mol Phys* 287(6):L1178–L1185
16. Polglase GR, Hooper SB, Gill AW, Allison BJ, Crossley KJ, Moss TJ, Nitsos I, Pillow JJ, Kluckow M (2010) Intrauterine inflammation causes pulmonary hypertension and cardiovascular sequelae in preterm lambs. *J Appl Physiol* 108(6):1757–1765
17. Romero R, Espinoza J, Goncalves LF, Gomez R, Medina L, Silva M, Chaiworapongsa T, Yoon BH, Ghezzi F, Lee W, Treadwell M, Berry SM, Maymon E, Mazor M, DeVore G (2004) Fetal cardiac dysfunction in preterm premature rupture of membranes. *J Matern Fetal Neonatal Med* 16(3):146–157
18. Seehase M, Gantert M, Ladenburger A, Garnier Y, Kunzmann S, Thomas W, Wirbelauer J, Speer CP, Kramer BW (2011) Myocardial response in preterm fetal sheep exposed to systemic endotoxaemia. *Pediatr Res* 70(3):242–246
19. Velten M, Hutchinson KR, Gorr MW, Wold LE, Lucchesi PA, Rogers LK (2011) Systemic maternal inflammation and neonatal hyperoxia induces remodeling and left ventricular dysfunction in mice. *PLoS One* 6(9):e24544
20. Yanowitz TD, Jordan JA, Gilmour CH, Towbin R, Bowen A, Roberts JM, Brozanski BS (2002) Hemodynamic disturbances in premature infants born after chorioamnionitis: association with cord blood cytokine concentrations. *Pediatr Res* 51(3):310–316
21. Holzapfel G, Gasser T, Ogden R (2000) A new constitutive framework for arterial wall mechanics and a comparative study of material models. *J Elast Phys Sci Solids* 61(1–3):1–48
22. Gasser TC, Schulze-Bauer CA, Holzapfel GA (2002) A three-dimensional finite element model for arterial clamping. *J Biomech Eng* 124(4):355–363

23. Rounioja S, Räsänen J, Glumoff V, Ojaniemi M, Mäkilä K, Hallman M (2003) Intra-amniotic lipopolysaccharide leads to fetal cardiac dysfunction. A mouse model for fetal inflammatory response. *Cardiovasc Res* 60(1):156–164
24. Tare M, Bensley JG, Moss TJ, Lingwood BE, Kim MY, Barton SK, Kluckow M, Gill AW, De Matteo R, Harding R, Black MJ, Parkington HC, Polglase GR (2014) Exposure to intrauterine inflammation leads to impaired function and altered structure in the preterm heart of fetal sheep. *Clin Sci (Lond)* 127(9):559–569
25. Macrae RA, Miller K, Doyle BJ (2016) Methods in mechanical testing of arterial tissue: a review. *Strain* 52(5):380–399
26. Humphrey JD (2002) Cardiovascular solid mechanics: cells, tissues and organs. Springer-Verlag, New York
27. Cox RH (1983) Comparison of arterial wall mechanics using ring and cylindrical segments. *Am J Phys* 244(2):H298–H303
28. Stoiber M, Messner B, Grasl C, Gschlad V, Bergmeister H, Bernhard D, Schima H (2015) A method for mechanical characterization of small blood vessels and vascular grafts. *Exp Mech* 55(8):1591–1595
29. Shazly T, Rachev A, Lessner S, Argraves W, Ferdous J, Zhou B, Moreira A, Sutton M (2015) On the uniaxial ring test of tissue engineered constructs. *Exp Mech* 55(1):41–51
30. Fung YC (1993) Biomechanics: mechanical properties of living tissues. Springer-Verlag, New York
31. Ogden RW (1972) Large deformation isotropic elasticity-on the correlation of theory and experiment for incompressible rubberlike solids. *Proc R Soc Lond A Math Phys Eng Sci* 326(1567):565–584
32. Booth AD, Wallace S, McEniery CM, Yasmin J, Brown D, Jayne R, Wilkinson IB (2004) Inflammation and arterial stiffness in systemic vasculitis: a model of vascular inflammation. *Arthritis Rheum* 50(2):581–588
33. Wallace SML, Mäki-Petäjä KM, Cheriyan J, Davidson EH, Cherry L, McEniery CM, Sattar N, Wilkinson IB, Kharbanda RK (2010) Simvastatin prevents inflammation-induced aortic stiffening and endothelial dysfunction. *Br J Clin Pharmacol* 70(6):799–806
34. Greenwald SE (2007) Ageing of the conduit arteries. *J Pathol* 211(2):157–172
35. Morris L, Wittek A, Miller K (2008) Compression testing of very soft biological tissues using semi-confined configuration—a word of caution. *J Biomech* 41(1):235–238

Computational Biomechanics for Medicine

From Algorithms to Models and Applications

Wittek, A.; Joldes, G.R.; Nielsen, P.M.F.; Doyle, B.; Miller, K. (Eds.)

2017, VIII, 173 p. 86 illus., 78 illus. in color., Hardcover

ISBN: 978-3-319-54480-9